View metadata, citation and similar papers at core.ac.uk

brought to you by CORE

provided by Elsevier - Publisher Connector

Biochimica et Biophysica Acta 1828 (2013) 2091–2098

Contents lists available at SciVerse ScienceDirect

Biochimica et Biophysica Acta

journal homepage: www.elsevier.com/locate/bbamem

Evaluation of membrane models and their composition for islet amyloid polypeptide-membrane aggregation

Lucie Caillon, Olivier Lequin, Lucie Khemtémourian *

UPMC Univ Paris 06, UMR 7203 CNRS-UPMC-ENS, Laboratoire des Biomolécules, 4 place Jussieu, 75005 Paris, France

ARTICLE INFO

Article history:
Received 31 October 2012
Received in revised form 26 April 2013
Accepted 13 May 2013
Available online 23 May 2013

Keywords:
Amyloid
IAPP
Model membranes (LUV SUV, bicelles, micelles)
Phospholipid
Aggregation kinetics
Fibril morphology

ABSTRACT

Human islet amyloid polypeptide (IAPP) forms amyloid fibrils in the pancreatic islets of patients suffering from type 2 diabetes mellitus (T2DM). The formation of IAPP fibrils has been shown to cause membrane damage which most likely is responsible for the death of pancreatic islet β-cells during the pathogenesis of T2DM. Several studies have demonstrated a clear interaction between IAPP and lipid membranes. However the effect of different lipid compositions and of various membrane mimetics (including micelles, bicelles, SUV and LUV) on fibril formation kinetics and fibril morphology has not yet systematically been analysed. Here we report that the interaction of IAPP with various membrane models promoted different processes of fibril formation. Our data reveal that in SDS and DPC micelles, IAPP adopts a stable α-helical structure for several days, suggesting that the micelle models may stabilize monomeric or small oligomeric species of IAPP. In contrast, zwitterionic DMPC/DHPC bicelles and DOPC SUV accelerate the fibril formation compared to zwitterionic DOPC LUV, indicating that the size of the membrane model and its curvature influence the fibrillation process. Negatively charged membranes decrease the lag-time of the fibril formation kinetics while phosphatidylethanolamine and cholesterol have an opposite effect, probably due to the modulation of the physical properties of the membrane and/or due to direct interactions with IAPP within the membrane core. Finally, our results show that the modulation of lipid composition influences not only the growth of fibrils at the membrane surface but also the interactions of β-sheet oligomers with membranes.

© 2013 Elsevier B.V. All rights reserved.

1. Introduction

Islet amyloid polypeptide (IAPP) is a 37-residue peptide hormone produced, stored and secreted together with insulin by the pancreatic β-cells. IAPP plays, in its soluble monomeric form, a role in the regulation of glucose homeostasis, in gastric emptying and in other cellular processes [1–4]. Human IAPP has a strong amyloidogenic propensity that has been linked to β-cell death in type 2 diabetes mellitus (T2DM) [5]. The amyloid deposits also named amyloid fibrils are composed of β-sheet aggregates with a characteristic structure similar to those found in Alzheimer's disease, Parkinson's disease, spongiform encephalopathy and a variety of other degenerative diseases [6–8].

It has been suggested that IAPP impairs the membranes of β-cells, leading to β-cell dysfunction and the development of T2DM [9,10]. It was proposed that this membrane disruption can be due to the growing IAPP fibrils [11] or to toxic oligomers [10,12,13]. Several studies have demonstrated a clear interaction between amyloid peptides and lipid membrane and have shown that membrane can modify the peptide structure and/or the kinetics of fibril formation [10,13–17]. It is noteworthy that the lipid systems used were often very simplistic models such as DPC micelles, SDS micelles, and vesicles containing phosphatidylcholine or a mixture of phosphatidylcholine and negatively charged lipids. In addition, comparison of published results is often hampered by the use of different systems and lipid compositions in various studies. Thus, it appears crucial to provide a critical assessment of the different membrane models used in the literature and to examine a larger number of membrane compositions to determine how a specific lipid composition or a specific membrane model could induce variation in the aggregation kinetics and fibril formation.

There is little information on the lipid compositions in pancreatic islets, but it was shown that phosphatidylcholine (PC) was the most abundant phospholipid class, followed by phosphatidylethanolamine (PE), sphingomyelin (SM) and phosphatidylserine (PS) [18,19]. In addition, it was shown that negatively charged membranes promote IAPP aggregation in vitro while the presence of cholesterol seems to

Abbreviations: CD, circular dichroism; DMSO, dimethyl sulfoxide; IAPP, human Islet Amyloid Polypeptide; HFIP, 1,1,1,3,3,3-hexafluoro-2-propanol; LUV, large unilamellar vesicle; DOPC, 1,2-dioleoyl-*sn*-glycero-3-phosphocholine; DOPS, 1,2-dioleoyl-*sn*-glycero-3-phospho-L-serine; DOPG, 1,2-dioleoyl-*sn*-glycero-3-phospho-(1′-*rac*-glycerol); DOPE, 1,2-dioleoyl-*sn*-glycero-3-phosphoethanolamine; DMPC, 1,2-dimyristoyl-*sn*-glycero-3-phosphocholine; DHPC, 1,2-dihexanoyl-*sn*-glycero-3-phosphocholine; DPPC, 1,2-dipalmitoyl-*sn*-glycero-3-phosphocholine; POPC, 1-palmitoyl-2-oleoyl-*sn*-glycero-3-phosphocholine; Chol, cholesterol; SM, sphingomyelin; SDS, sodium dodecyl sulphate; DPC, dodecyl phosphocholine; ThT, Thioflavin T

* Corresponding author. Tel.: +33 1 44 27 31 15; fax: +33 1 44 27 38 43.
E-mail address: lucie.khemtemourian@upmc.fr (L. Khemtémourian).

0005-2736/$ – see front matter © 2013 Elsevier B.V. All rights reserved.
http://dx.doi.org/10.1016/j.bbamem.2013.05.014

slow down the aggregation [14,20]. Thus, we incorporated these components (PC, PE, PS, SM and Chol) as well as phosphatidylglycerol (PG) into our model lipid system in proportions that represent a consensus between previous studies and data in literature.

To gain further insight into the potential importance of lipid composition we performed a biophysical study of IAPP in lipid bilayers of different compositions and in various membrane models (including micelles, bicelles, SUV and LUV). In particular, we examined the structure, the aggregation behaviour and the fibril morphology of IAPP. The vesicles made from the predominant plasma membrane phospholipid (phosphatidylcholine) were used as our core model membrane to which other lipids were added. In total, the aggregation of IAPP was studied in 16 membrane models of different compositions. The different lipid systems used to induce IAPP aggregation showed different kinetic parameters and most of them except the micelles showed fine fibril structures all consistent with β-sheet aggregates.

2. Materials and methods

2.1. Materials

The synthesis of human IAPP with an amidated C-terminus and disulfide bridge was performed using Fmoc chemistry at the Institut de Biologie Intégrative (IFR83-Université Pierre et Marie Curie). The peptide was purified by reverse phase high-performance liquid chromatography (HPLC). Purity of peptide was higher than 95% as determined by analytical HPLC and peptide identity was confirmed by MALDI-TOF mass spectrometry. Its amino acid sequence is: KCNTATCATQRLANFLVHSSNNFGAILSSTNVGSNTY. DOPC, POPC, DMPC, DOPE and cholesterol (obtained from Genzyme, Switzerland) and DPC, DOPS, DOPG, DPPC and SM (obtained from Avanti Polar Lipids, Alabaster, USA) were used without further purification. SDS and Thioflavin T (ThT) were obtained from Sigma.

2.2. Preparation of peptide samples

An essential criterion for measuring aggregation kinetics of amyloid peptides and thus the effect of phospholipids is to start with a monomeric form of the peptide. Therefore, peptide stock solutions were freshly prepared prior to all experiments using the same batch. Peptide was dissolved at a concentration of 1 mM in hexafluoro-isopropanol (HFIP) and incubated for at least 1 h. Next, HFIP was evaporated, followed by vacuum desiccation for at least 1 h. For the ThT fluorescence and the microscopy experiments, the peptide film was then dissolved in DMSO to a final peptide concentration of 0.2 mM. For those experiments, we used the same concentration of DMSO (5% in the final volume) and hence we were able to compare the shape of the curve and the lag-time. For the CD experiments, the resulting peptide film was solubilized by addition of a dispersion of LUV, bicelles or micelles in 10 mM sodium phosphate buffer, pH 7.4.

2.3. Preparation of large unilamellar vesicles (LUV)

Each lipid system was prepared by dissolving the desired lipids in chloroform or chloroform/methanol (3:1) in a glass tube. The solvent was evaporated with dry nitrogen gas yielding a lipid film that was subsequently kept in a vacuum desiccator for 30 min. Lipid films were hydrated for at least 30 min in 10 mM Tris/HCl, 100 mM NaCl, pH 7.4 for the fluorescence and microscopy experiments and in 10 mM sodium phosphate buffer, pH 7.4 for the CD experiments. The lipid suspensions were subjected to 10 freeze–thaw cycles, at temperatures of approximately −190 °C and 50 °C, respectively, and subsequently extruded 19 times through a mini-extruder (Avanti Alabaster, AL) equipped with polycarbonate membranes (at 50, 200 and 800 nm cut-off). The phospholipid content of lipid stock solutions and vesicle preparations was determined by assessing inorganic phosphate according to Rouser [21].

2.4. Preparation of SDS and DPC micelles and DMPC/DHPC bicelles

Micelles of SDS and DPC were obtained by dissolving SDS or DPC in appropriate buffer to a final concentration of 10 mM (above the cmc). Bicelles were prepared according to Raffard et al. [22] by hydrating DMPC and DHPC with appropriate buffer to a final concentration of 10 mM DHPC and 5 mM DMPC. The mixture was then submitted three times to the following cycle: 5 min of centrifugation at 4000 rpm, vigorous vortexing, freezing in liquid nitrogen, heating in a 50 °C water bath, vigorous vortexing.

2.5. CD spectroscopy

CD spectra were measured on a Jasco 815 spectropolarimeter (Jasco Inc., Easton, MD) over the wavelength range 190–260 nm, by using 0.1 cm path length quartz cell (internal volume 200 μL) from Hellma GmbH. CD spectra were recorded at 25 °C, at 0.2 nm intervals and 10 $nm \cdot min^{-1}$ scan speed. Measurements were carried out in 10 mM phosphate buffer at pH 7.4. Peptide concentrations were 25 μM in the presence of lipids (peptide:lipid ratio 1:20) or in the presence of detergents (10 mM SDS or DPC). To follow IAPP conformational changes, spectra were recorded at regular intervals and the CD signal at 220 nm was plotted vs. time of incubation. Experimental values were fitted to a Boltzmann sigmoidal equation:

$$\theta_{220} = \frac{\theta_i - \theta_f}{1 + e^{(t - t0.5)/dt}} + \theta_f.$$

In this equation, θ_i and θ_f are the initial and final ellipticity values at 220 nm, $t_{0.5}$ is the time to 50% of transition conformational and dt a time constant. The CD experiments were performed 2 times on different days using different IAPP stock solutions and different vesicles.

2.6. Thioflavin T assays

The kinetics of fibril formation were measured using the fluorescence intensity increase upon binding of the fluorescent dye Thioflavin T (ThT) to fibrils. A plate reader (Fluostar Optima, Bmg Labtech) and standard 96-well flat-bottom black microtiter plates in combination with a 440 nm excitation filter and a 485 nm emission filter were used. The ThT assay was started by adding 10 μL of a 0.2 mM IAPP solution in DMSO to 190 μL of a mixture of 10 μM ThT, LUV (peptide concentration: 10 μM peptide; 200 μM lipid; 10 mM detergent) and 10 mM Tris/HCl, 100 mM NaCl, pH 7.4. The microtiter plate was shaken for 10 s directly after addition of all components, but not during the measurement. The ThT assay was performed 3 times, each in triplicate, on different days, using different IAPP stock solutions. The replicates of each system showed fairly consistent reproducibility.

2.7. Electron microscopy

Peptide and vesicles were incubated under the same conditions as in the Thioflavin T assay. Aliquots (25 μL) of this mixture were adsorbed onto glow-discharged carbon-coated 300-mesh copper grids for 2 min. Grids were then blotted and dried. Grids were negatively stained for 45 s on 2% uranyl acetate, blotted and dried. Grids were examined using a ZEISS 912 Omega electron microscope operating at 80 kV. The samples were prepared and observed 2 times using different IAPP and vesicles stocks.

3. Results

3.1. Preparation of IAPP and membrane models

To evaluate the role of the lipid composition as well as the membrane models on IAPP aggregation, we performed a systematic study using circular dichroism, fluorescence and microscopy. An essential criterion for measuring and comparing aggregation kinetics of IAPP on the different membrane models is to start with a monomeric form of the peptide. Indeed, amyloid peptides are known to produce variable results due to preformed oligomers acting as seeds. Therefore, the IAPP peptide stocks were always made fresh and preincubated in HFIP, a treatment that was shown to lead to monomeric species essentially [23]. The experiments were performed in triplicate and 16 membrane models were tested for this study including detergent micelles, bicelles, small unilamellar vesicles (SUV) and large unilamellar vesicles (LUV). Detergent micelles commonly consist of amphiphiles such as dodecylphosphocholine (DPC) or sodium dodecyl sulphate (SDS). The detergent head groups may be designed to physically mimic the surface of a biological membrane. However, a micelle typically contains 50–80 detergent molecules; serious concerns arise regarding the very small radius of curvature and the lack of a true lipid bilayer. Consequently, the study was also performed using bicelles, which are formed by mixing long-chain and short-chain phospholipids [24]. The bicelle interior consists of a true lipid bilayer, while the short-chain phospholipid is believed to be sequestered to the rim of the disks. Under our conditions of temperature, hydration, and lipid ratios, the mixtures were reported to form fast-tumbling bicelles also named isotropic bicelles. Finally, LUV from diverse compositions and SUV were used to examine the role of the phospholipids and of the liposome size in IAPP fibril formation.

3.2. IAPP undergoes a conformational rearrangement depending on the membrane composition

We previously showed that the conformation of IAPP in solution and in the presence of membranes changes within a few hours from random coil/α-helical conformation to β-sheet structure, indicative of amyloid fibrils [25]. The conformational studies on IAPP on different membrane models were conducted by recording CD spectra in the range 190–260 nm at 30 min intervals in phosphate buffer without sodium chloride so as to increase the signal-to-noise ratio, keeping in mind that the absence of salt may slow down the β-sheet transition [26]. In the presence of SDS micelles (Fig. 1A), the spectrum of IAPP displays negative ellipticity at 208 and 222 nm, characteristic of an α-helical backbone structure. After a few days of incubation, IAPP retains its α-helical conformation and shows no evidence of β-sheet structure that would indicate fibril formation. Similar results were observed with DPC micelles (data not shown). Surprisingly, in the presence of DMPC/DHPC zwitterionic bicelles (Fig. 1B), IAPP adopts initially an α-helical structure but converts rapidly in around 2–3 h to β-sheet structure, suggesting the formation of fibrils.

It was already shown that upon interaction with membranes containing negatively charged lipids, IAPP adopts an α-helical conformation, which in time undergoes a transition to β-sheet. The spectrum of IAPP in DOPC/DOPS (7:3) LUV in Fig. 1C confirms this behaviour. The α-helical to β-sheet transition occurs after 30 min. Similar results were observed in DOPC/DOPG (7:3) LUV with a transition time of approximately 60 min (data not shown).

In all other CD spectra, IAPP freshly added to the membrane models displayed typical random coil conformation with minima at 200 nm corresponding to the non-amyloidogenic conformation of monomeric or small soluble IAPP. After a few hours of incubation, the CD spectra

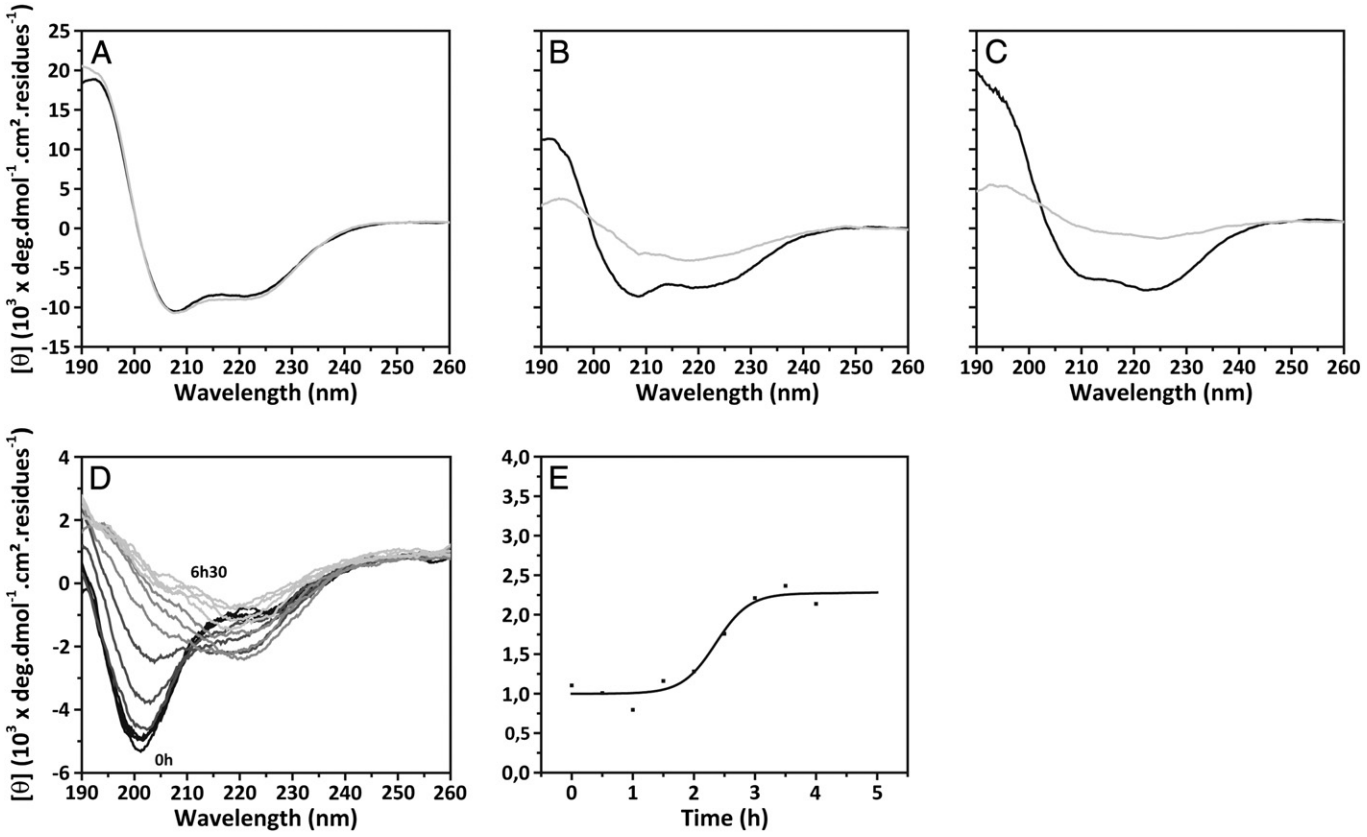

Fig. 1. CD spectra (190–260 nm) of IAPP (20 μM) freshly dissolved (black) and after 24 h of incubation (grey) in (A) SDS micelles, (B) DHPC/DMPC bicelles, and (C) DOPC/DOPS (7:3) LUV. (D) CD kinetic study in DMPC LUVs. Overlaid CD spectra recorded at 30 min intervals. Plot color code: black: CD spectrum recorded after 5 min, light grey: CD spectrum recorded after 6 h30. (E) Time course of CD ellipticity at 220 nm.

undergo a typical change to β-sheet secondary structure with a minimum around 220 nm, characteristic of the amyloidogenic conformation. In Fig. 1D the overlaid CD spectra of IAPP in DMPC LUV show the conformation transition from the random coil to the β-sheet structure. The prevalence of β-sheet secondary structure after 3 h is clearly indicated by the appearance of a negative band at 220 nm and the loss of the negative band at 200 nm. By plotting the CD value at 220 nm against time, a sigmoid curve, in agreement with previous reports [27,28], is obtained and is characterized by three steps: a lag phase, an exponential growth phase and a plateau (Fig. 1E). During the first step, IAPP retains its random coil conformation, then an exponential increase in β-sheet content is observed and finally the plateau defined the beginning of fibril formation. Extended incubation time caused the CD signal to decrease proving that IAPP was becoming insoluble. The time required to reach half-value of the maximum CD signal at 220 nm ($t_{0.5}$), reported in Table 1, is used to compare the lag time of the sigmoidal transitions of the kinetic curves of CD experiments in different membrane models. Depending on the membrane models, the random coil to β-sheet transition occurs between 2 to 16 h (Table 1). As a reference, the lipid-free system presented a transition time of 9.7 ± 0.1 h and an elongation rate of 1.3 ± 0.1 h^{-1}. DMPC LUV provided the shortest random coil to β-sheet transition time (2.4 ± 0.1 h) but the slowest elongation rate (0.3 ± 0.1 h^{-1}). In contrast, DPPC LUV presented the longest conformational transition time (15.6 ± 0.4 h) with slightly slower elongation rate (0.6 ± 0.3 h^{-1}) than DOPC LUV (0.9 ± 0.1 h^{-1}). The vesicles containing cholesterol (DOPC/Chol, DOPC/Chol/SM and POPC/Chol/SM) produced an increase in conformational transition time and a decrease in elongation rate while adding 30% of sphingomyelin without cholesterol slightly reduced the transition time to 8.6 ± 0.1 h and promoted a slower elongation rate (0.5 ± 0.1 h^{-1}). Larger size DOPC vesicles (800 nm) induced no change in the transition time, neither in the elongation rate compared to 200 nm DOPC. However, 50 nm DOPC SUV and DOPC/DOPE LUV provided a short transition time (7.4 ± 0.1 h and 7.8 ± 0.1 h respectively) and a slow elongation rate (0.6 ± 0.1 $h^{-1}$and 0.4 ± 0.1 h^{-1}). Overall, our CD data show that the transition from α-helical to β-sheet or from random coil to β-sheet is observed in all system but micelles. In these latter models, the α-helical structure is stable for several days, suggesting the absence of fibril formation.

3.3. Effects of membrane composition and membrane size on IAPP fibril formation

To examine whether indeed IAPP amyloid fibrils are formed in all systems but micelles, we used the complementary approach of measuring fluorescence intensity changes upon binding the amyloid specific dye Thioflavin T (ThT), which is a commonly used method to detect amyloid fibrils [29]. Fig. 2 shows typical S-shaped curves characteristic of amyloid fibril formation [23], obtained for IAPP in different membrane models, except the micelles (Fig. 2B open square and cross). Table 2 represents the time required to reach half-value of the maximum ThT signal ($t_{0.5}$), and is used to compare the lag time of the sigmoidal transitions in the kinetic curves of ThT-fluorescence experiments in different membrane models. Depending on the membrane models, the monomer/small soluble oligomers to fibril formation transition occurs between 2 to 20 h (Table 2). The lipid-free system showed a transition time of 9.7 ± 1.0 h and an elongation rate of 1.5 ± 0.2 h^{-1}. In DOPC/DOPS (7:3) and DOPC/DOPG (7:3), the lag time is approximately 2 h while in DOPC only and in DOPC/DOPE the lag time reaches 12 h and 21 h, respectively (Fig. 2A). These results indicate that the presence of negatively charged lipids largely accelerates the fibril formation while the presence of the zwitterionic phosphatidylethanolamine slows down the fibril formation. Next, the role of the membrane models and vesicles size was examined using SDS and DPC micelles, DMPC/DHPC bicelles, 50 nm SUV and 800 nm LUV. As shown in Fig. 2B, analysis of the kinetics of fibril formation in the presence of DMPC/DHPC bicelles, SUV and LUV yields the typical S-shaped curve for IAPP. In addition, the lag time is shorter in bicelles and SUV (~7–9 h) than that in 800 nm LUV (~16 h), suggesting that IAPP-fibril formation might be favoured by small membrane with high curvature. In contrast, the data do not show any increase in time in fluorescence for IAPP in DPC and in SDS micelles, supporting the notion that in these media IAPP is not fibrillogenic under the same experimental conditions. These results suggest that the micelles stabilize a monomeric form of IAPP and that the size of the membrane mimetics and their curvature influence the fibrillation process. Then, the role of the length of the lipid chains as well as the degree of unsaturation was examined using DMPC, DPPC and POPC LUV. Our results show a quite similar profile of kinetics of IAPP-fibril formation in these vesicles with a lag-time of 11–15 h (Fig. 2C) suggesting that the lipid chains have a slight effect on fibril formation. Finally, the kinetics of IAPP fibril formation was studied in the presence of cholesterol and sphingomyelin (Fig. 2D). These two lipids are components of lipid microdomains, also called lipid rafts, and are considered to be a platform of a large number of events in plasma membrane [30–32]. Thus, we performed ThT-fluorescence experiments using the following vesicles: DOPC/Chol (7:3), DOPC/SM (7:3), DOPC/Chol/SM 4:3:3 and POPC/Chol/SM 1:1:1. Our results show that fibrils are formed more slowly in the presence of cholesterol while sphingomyelin does not seem to have a specific effect on the kinetics of fibril formation.

Table 1
Kinetic parameters (lag time $t_{0.5}$ and elongation rate dt) of IAPP β-sheet formation in the different media determined using the time course of absolute CD ellipticity at 220 nm.

Membranes	$t_{0.5}$ (h)	dt (h^{-1})
Lipid-free	9.7 ± 0.1	1.3 ± 0.1
DOPC	**8.9 ± 0.1**	**0.9 ± 0.1**
DOPC/DOPE (7:3)	7.8 ± 0.1	0.4 ± 0.1
DOPC 50 nm	7.4 ± 0.1	0.6 ± 0.1
DOPC 800 nm	8.5 ± 0.1	0.8 ± 0.1
DMPC	2.4 ± 0.1	0.3 ± 0.1
DPPC	15.6 ± 0.4	0.6 ± 0.3
POPC	6.1 ± 0.3	0.7 ± 0.3
DOPC/SM (7:3)	8.6 ± 0.1	0.5 ± 0.1
DOPC/Chol (7:3)	10.0 ± 0.2	0.4 ± 0.2
DOPC/Chol/SM (4:3:3)	11.9 ± 1.0	0.7 ± 0.6
POPC/Chol/SM (1:1:1)	14.4 ± 0.3	1.0 ± 0.2

3.4. Fibril morphology upon incubation with the different lipid systems

Finally, the amyloid fibrils were examined by TEM, revealing that the morphology of the fibrils was particular to the lipid system (Fig. 3A–P). In solution (data not shown) and for all the LUV and SUV, the fibrils exhibited the typical morphology of long and twist amyloid fibrils with widths between 10 and 15 nm. Interestingly, the fibrils seemed to propagate along the vesicle's surface and distorted vesicles (asterisks in Fig. 3H) are present near the IAPP fibrils (black arrows in Fig. 3H). In SDS and DPC micelles, no fibrils were found even after several days of incubation (Fig. 3E–F). These results are consistent with our ThT fluorescence and CD data that respectively show no increase in ThT signal after few hours of incubation, and predominantly α-helical structure during several days of incubation. Thus, our TEM results suggest that in SDS and DPC micelles the peptide is not fibrillogenic. In DHPC/DMPC bicelles, fibrils were observed after a few hours of incubation in agreement with our CD data and ThT experiments. However, the morphology of these fibrils is different from the one in the LUV (Fig. 3G). Indeed, the populations of IAPP fibrillar assemblies in the bicelles consist of thinner structures than in other vesicles with widths between 8 and 12 nm.

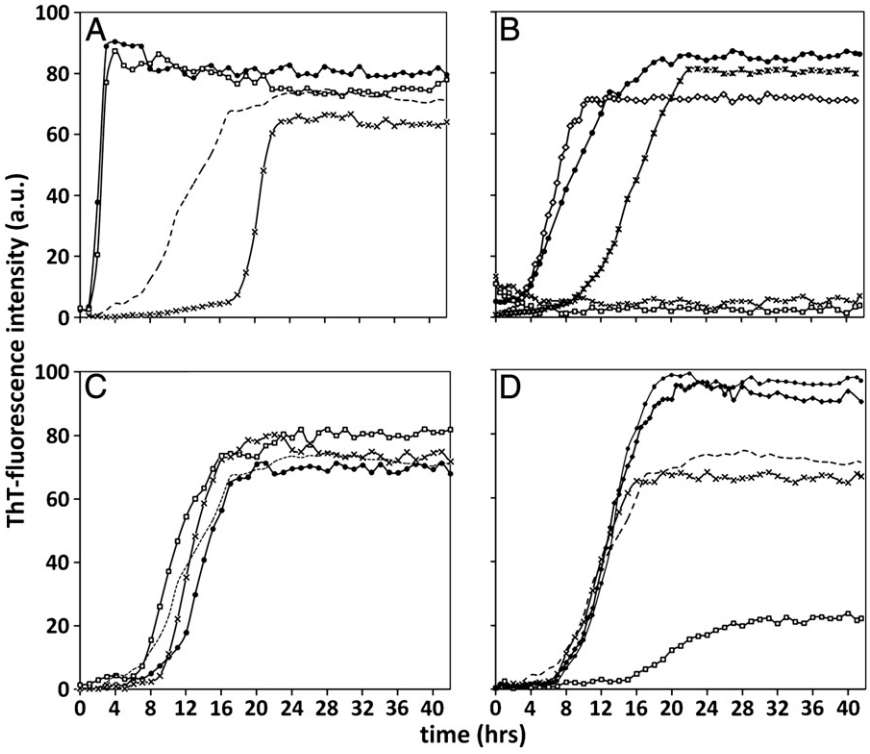

Fig. 2. Monitoring the IAPP-fibril formation by ThT fluorescence in the presence of (A) DOPC (dash), DOPC/DOPS 7:3 (filled circles), DOPC/DOPG 7:3 (open squares), DOPC/DOPE 7:3 (cross); (B) DMPC/DHPC bicelles (filled circles), SDS micelles (open squares), DPC (cross) micelles, DOPC 50 nm SUV (open diamonds) and DOPC 800 nm LUVs (stars); (C) DOPC (dot), DMPC (open squares), POPC (filled circle) and DPPC (cross); (D) DOPC (dash), DOPC/Chol 7:3 (open squares), DOPC/SM 7:3 (cross), DOPC/Chol/SM 4:3:3 (filled circles) and POPC/Chol/SM 1:1:1 (filled diamonds).

4. Discussion

In vitro studies on model membranes have shown that membrane permeabilization by amyloidogenic peptides is highly dependent on the lipid composition of the membrane [14,33]. Therefore, an understanding of lipid specificity of amyloid peptide–lipid interactions can lead to a better understanding of the mechanisms of amyloid cytotoxicity. In the present study we have investigated and compared the aggregational behaviour of IAPP in lipid membrane models of different compositions and sizes. We have made the following key observations: i) SDS and DPC micelles stabilize α-helical conformations and no IAPP fibril formation was observed in these media; ii) DMPC/DHPC bicelles and DOPC SUV tend to accelerate IAPP fibril formation; iii) the headgroup of the lipid strongly influences the kinetics of amyloid formation, as revealed by ThT-fluorescence; the length and the degree of unsaturation of the lipid chains have little effect on the fibril formation as assessed by ThT fluorescence but affect peptide β-sheet transition as observed by CD; iv) lipid rafts containing cholesterol tend to retard IAPP fibril formation. These findings are discussed below.

Table 2
Kinetic parameters (lag time $t_{0.5}$ and elongation rate dt) of IAPP fibril formation in the different media determined using ThT-fluorescence.

Membranes	$t_{1/2}$ (h)	dt (h^{-1})
Lipid-free	9.7 ± 1.0	1.5 ± 0.2
DOPC	**11.8 ± 1.2**	**2.6 ± 0.2**
DOPC/DOPS	2.1 ± 0.5	0.2 ± 0.2
DOPC/DOPG	2.2 ± 0.5	0.2 ± 0.2
DOPC/DOPE (7:3)	20.2 ± 2.0	0.8 ± 0.2
DOPC 50 nm	6.3 ± 0.8	1.3 ± 0.2
DOPC 800 nm	15.5 ± 1.5	2.3 ± 0.2
DMPC	10.7 ± 1.2	2.1 ± 0.2
DPPC	12.3 ± 1.2	1.3 ± 0.2
POPC	13.6 ± 1.2	1.6 ± 0.2
DOPC/Chol (7:3)	20.1 ± 2.0	2.9 ± 0.2
DOPC/SM (7:3)	13.1 ± 1.8	1.6 ± 0.2
DOPC/Chol/SM (4:3:3)	13.1 ± 1.2	1.6 ± 0.2
POPC/Chol/SM (1:1:1)	12.9 ± 1.3	2.4 ± 0.2
Bicelles	8.5 ± 0.8	2.8 ± 0.2

The CD, TEM and ThT fluorescence studies of IAPP in micelles reveal several interesting features. No fibrils were found in these media after several days of incubation, consistent with our ThT fluorescence and CD data that show no increase in ThT signal after 2 days of incubation, and predominantly α-helical structure for several days in both anionic and zwitterionic micelles. It appears reasonable to suggest that micelles inhibit fibril formation of IAPP and may stabilize a monomeric form or small soluble oligomeric forms of IAPP that exhibit mainly α-helical conformations. The micelles models are thus suitable to characterize the solution conformation of IAPP as was done by the group of Ramamoorthy, which solved the high-resolution structure of IAPP in SDS micelles using NMR [34,35]. Similarly, Aβ peptide, aggregating in Alzheimer's disease has also been studied in DPC micelles and SDS micelles [36,37]. Interestingly, our experiments in small isotropic DHPC/DMPC bicelles and SUV show that these media promote IAPP fibril formation within a few hours. These two mimetics are considered as better models than micelles, since the composition and conditions can be varied to better reproduce specific biological membranes [38]. Our study clearly demonstrates that small isotropic bicelles and SUV are appropriate for studying the membrane interactions of amyloidogenic peptides such as IAPP. Small isotropic bicelles in particular are amenable to high resolution solution NMR studies so the structure of IAPP species bound to membranes could be determined using such mimetics. Noteworthy, the fibrils formed in the presence of small isotropic bicelles show slightly altered morphology with thinner structures. This may indicate that the bicelle environment provides a limited area to accommodate IAPP oligomers on the membrane surface during the nucleation process.

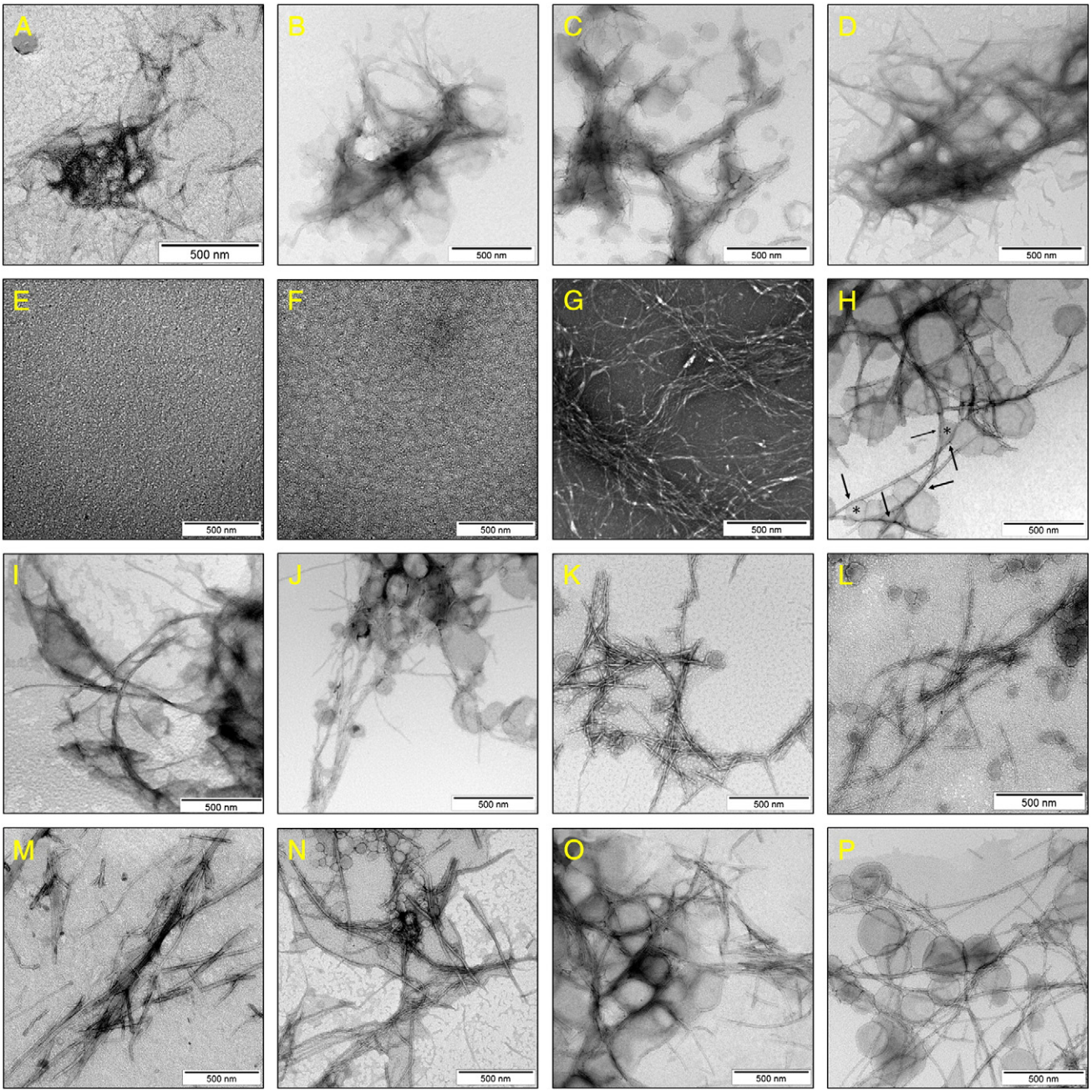

Fig. 3. Negatively stained microscopy images of IAPP after incubation of 24 h with vesicles composed of: (A) DOPC, (B) DOPC/DOPS 7:3, (C) DOPC/DOPG 7:3, (D) DOPC/DOPE 7:3, (E) with SDS micelles, (F) DPC micelles, (G) DMPC/DHPC bicelles, (H) with DOPC SUV (50 nm), (I) DOPC 800 nm, (J) DMPC, (K) DPPC (L) POPC, (M)DOPC/Chol 7:3, (N) DOPC/SM 7:3,(O) DOPC/Chol/SM 4:3:3and (P) POPC/Chol/SM 1:1:1. All SUV and LUV incubated experiments had a 1:20 peptide to lipid molar ratio. Scale bars represent 500 nm.

Upon interaction with negatively charged lipids (PS and PG), IAPP adopts an α-helical structure, in agreement with previous reports [14,39]. A transition of α-helical to β-sheet structure is observed, that results in fibril formation. This α-helical to β-sheet transition has also been observed for many amyloidogenic proteins, such as Aβ peptide and the N-terminal part of α-synuclein (aggregating in Parkinson's disease) [40,41]. In addition, our results show that negatively charged lipids accelerate IAPP-fibril formation while they appeared to slow down Aβ-fibril formation [42]. These diverging kinetics effects can be related to the different isoelectric points of Aβ and IAPP peptides that exhibit negative and positive charges, respectively, at neutral pH. Our data indicate that the net surface charge is an important property of the membrane that strongly affects the kinetics of amyloid formation, however no noticeable difference was observed between phosphatidylserine and phosphatidylglycerol anionic headgroups.

In the presence of the zwitterionic phosphatidylethanolamine, a different behaviour was observed: the kinetics of fibril formation is slower (with a lag-time of approximately 21 h) while the α-helical to β-sheet transition, as observed by CD, occurs faster, after few hours. It is important to keep in mind that the ThT-fluorescence was performed in the presence of salt, which should even accelerate the kinetics of fibril formation, while the CD experiments performed without salt should retard the kinetics of conformational change. Thus, the diverging kinetics followed by ThT fluorescence and CD spectroscopy suggest that the presence of phosphatidylethanolamine stabilizes some oligomeric β-sheet-structures of IAPP but slows down IAPP-fibril formation. It was recently proposed that IAPP oligomers are prone to form on the membrane surface and that phosphatidylethanolamine may indeed favour the formation of oligomers by increasing the amount of membrane-bound IAPP [43,44]. The comparison of models yields

information on the effect of bilayer curvature on IAPP fibril formation process. The kinetics is slowed down in the presence of PE which has a negative curvature while SUV exhibiting a positive curvature tend to accelerate fibril formation.

The length and the degree of unsaturation of the lipid chains have little effect on the fibril formation but affect the transition from the non-amyloidogenic conformation (random coil) of monomeric IAPP and small soluble oligomers to the β-sheet-rich conformation. Indeed, our results show that DPPC LUV presented the longest conformational transition time compared to DOPC, DMPC and POPC LUV. Importantly, at this temperature (25 °C) DPPC is in ordered (gel) lipid phase, which induces change in the structural characteristics and dynamics properties of the membranes. Thus, we might assume that the peptide has difficulty to insert in the bilayer due to the ordered phase that may retard the random coil to β-sheet transition.

The addition of sphingomyelin in the membrane models did not show any effect on IAPP-fibril morphology neither on fibril formation with similar lag-time of approximately 12 h in both systems. This was unexpected since previous results on Aβ peptide, show a clear interaction between Aβ and several sphingolipids and in vivo experiments demonstrate that sphingomyelin is critical in Aβ-amyloid fibrillation in the brain [45].

The role of cholesterol in amyloid disease development is unclear, as the literature data show contradictory results indicating either that cholesterol has a protective effect against membrane permeabilization or that cholesterol is impairing the membrane stability [46–49]. The exact role of cholesterol in IAPP fibril formation and membrane damage is currently in question. Our CD and ThT-fluorescence results show that the vesicles containing 30% of cholesterol (i.e., DOPC/Chol 7:3) slow down the kinetics of oligomer formation as well as of IAPP-fibril formation. The cholesterol effects could be due to the modulation of the physical properties of the membrane and/or due to direct interactions with IAPP within the membrane core. Indeed, cholesterol is a known regulator of membrane fluidity. It is therefore quite possible that cholesterol, by modulating membrane fluidity and/or membrane curvature, also influences IAPP–lipid interaction and reduces IAPP-fibril formation.

In conclusion, our data indicate that the lipid composition of vesicles has a large effect on IAPP-fibril formation by accelerating or slowing down the kinetics, but has only slight effects on the morphology of final amyloid fibrils, as observed by EM. It is important to note that the fibrils morphology is the same in the absence and in the presence of lipid vesicles. Membrane models also affect the kinetics of β-sheet conformational transition and of amyloid fibril formation to different extents. It is therefore likely that the modulation of lipid composition influences not only the interactions of β-sheet oligomers with membranes but also the growth of fibrils at the membrane surface. Thus, the discrepancy of results found in the literature is most likely due to variation of lipid compositions and membrane models used by the authors.

Acknowledgements

Christophe Piesse and Géraldine Toutirais (IFR83-Université Pierre et Marie Curie, France) are acknowledged for the amyloid peptide synthesis and the electron microscopy, respectively. We thank the students who participated on the projects, Julia Petit and Alice Bouige.

References

[1] B. Akesson, G. Panagiotidis, P. Westermark, I. Lundquist, Islet amyloid polypeptide inhibits glucagon release and exerts a dual action on insulin release from isolated islets, Regul. Pept. 111 (2003) 55–60.
[2] E. Karlsson, IAPP as a regulator of glucose homeostasis and pancreatic hormone secretion (review), Int. J. Mol. Med. 3 (1999) 577–584.
[3] T.K. Reda, A. Geliebter, F.X. Pi-Sunyer, Amylin, food intake, and obesity, Obes. Res. 10 (2002) 1087–1091.
[4] P.A. Rushing, M.M. Hagan, R.J. Seeley, T.A. Lutz, D.A. D'Alessio, E.L. Air, S.C. Woods, Inhibition of central amylin signaling increases food intake and body adiposity in rats, Endocrinology 142 (2001) 5035.
[5] J.W.M. Höppener, B. Ahrén, C.J. Lips, Islet amyloid and type 2 diabetes mellitus, N. Engl. J. Med. 343 (2000) 411–419.
[6] F. Chiti, C.M. Dobson, Protein misfolding, functional amyloid, and human disease, Annu. Rev. Biochem. 75 (2006) 333–366.
[7] D.J. Selkoe, Folding proteins in fatal ways, Nature 426 (2003) 900–904.
[8] J.D. Sipe, Amyloidosis, Crit. Rev. Clin. Lab. Sci. 31 (1994) 325–354.
[9] J.W. Höppener, C.J. Lips, Role of islet amyloid in type 2 diabetes mellitus, Int. J. Biochem. Cell Biol. 38 (2006) 726–736.
[10] L. Khemtémourian, J.A. Killian, J.W.M. Höppener, M.F.M. Engel, Recent insights in islet amyloid polypeptide-induced membrane disruption and its role in beta-cell death in type 2 diabetes mellitus, Exp. Diabetes Res. 2008 (2008) 421287.
[11] M.F.M. Engel, L. Khemtémourian, C.C. Kleijer, H.J. Meeldijk, J. Jacobs, A.J. Verkleij, B. de Kruijff, J.A. Killian, J.W.M. Höppener, Membrane damage by human islet amyloid polypeptide through fibril growth at the membrane, Proc. Natl. Acad. Sci. U. S. A. 105 (2008) 6033–6038.
[12] R. Kayed, E. Head, J.L. Thompson, T.M. McIntire, S.C. Milton, C.W. Cotman, C.G. Glabe, Common structure of soluble amyloid oligomers implies common mechanism of pathogenesis, Science 300 (2003) 486–489.
[13] M.F.M. Engel, Membrane permeabilization by Islet Amyloid Polypeptide, Chem. Phys. Lipids 160 (2009) 1–10.
[14] J.D. Knight, A.D. Miranker, Phospholipid catalysis of diabetic amyloid assembly, J. Mol. Biol. 341 (2004) 1175–1187.
[15] J. Janson, R.H. Ashley, D. Harrison, S. McIntyre, P.C. Butler, The mechanism of islet amyloid polypeptide toxicity is membrane disruption by intermediate-sized toxic amyloid particles, Diabetes 48 (1999) 491–498.
[16] E. Sparr, M.F.M. Engel, D.V. Sakharov, M. Sprong, J. Jacobs, B. de Kruijff, J.W.M. Höppener, J.A. Killian, Islet amyloid polypeptide-induced membrane leakage involves uptake of lipids by forming amyloid fibers, FEBS Lett. 577 (2004) 117–120.
[17] T.L. Lau, J.D. Gehman, J.D. Wade, C.L. Masters, K.J. Barnham, F. Separovic, Cholesterol and clioquinol modulation of A beta(1-42) interaction with phospholipid bilayers and metals, Biochim. Biophys. Acta 1768 (2007) 3135–3144.
[18] A. Hallberg, Effects of starvation and different culture conditions on the phospholipid content of isolated pancreatic-islets, Biochim. Biophys. Acta 796 (1984) 328–335.
[19] J. Seeliger, K. Weise, N. Opitz, R. Winter, The effect of Abeta on IAPP aggregation in the presence of an isolated beta-cell membrane, J. Mol. Biol. 421 (2012) 348–363.
[20] W.J. Cho, S. Trikha, A.M. Jeremic, Cholesterol regulates assembly of human islet amyloid polypeptide on model membranes, J. Mol. Biol. 393 (2009) 765–775.
[21] G. Rouser, S. Fkeischer, A. Yamamoto, Two dimensional then layer chromatographic separation of polar lipids and determination of phospholipids by phosphorus analysis of spots, Lipids 5 (1970) 494–496.
[22] G. Raffard, S. Steinbruckner, A. Arnold, J.H. Davis, E.J. Dufourc, Temperature–composition diagram of dimyristoylphosphatidylcholine-dicaproylphosphatidylcholine "bicelles" self-orienting in the magnetic field. A solid state H-2 and P-31 NMR study, Langmuir 16 (2000) 7655–7662.
[23] S.B. Padrick, A.D. Miranker, Islet amyloid: phase partitioning and secondary nucleation are central to the mechanism of fibrillogenesis, Biochemistry 41 (2002) 4694–4703.
[24] N.E. Gabriel, M.F. Roberts, Spontaneous formation of stable unilamellar vesicles, Biochemistry 23 (1984) 4011–4015.
[25] L. Khemtémourian, E. Domenech, J.P.F. Doux, M.C. Koorengevel, J.A. Killian, Low pH acts as inhibitor of membrane damage induced by human islet amyloid polypeptide, J. Am. Chem. Soc. 133 (2011) 15598–15604.
[26] P.J. Marek, V. Patsalo, D.F. Green, D.P. Raleigh, Ionic strength effects on amyloid formation by amylin are a complicated interplay among Debye screening, ion selectivity, and Hofmeister effects, Biochemistry 51 (2012) 8478–8490.
[27] Y. Fezoui, D.B. Teplow, Kinetic studies of amyloid beta-protein fibril assembly. Differential effects of alpha-helix stabilization, J. Biol. Chem. 277 (2002) 36948–36954.
[28] M. Bartolini, C. Bertucci, M.L. Bolognesi, A. Cavalli, C. Melchiorre, V. Andrisano, Insight into the kinetic of amyloid beta (1-42) peptide self-aggregation: elucidation of inhibitors' mechanism of action, Chembiochem 8 (2007) 2152–2161.
[29] H. LeVine III, Quantification of beta-sheet amyloid fibril structures with thioflavin T, Methods Enzymol. 309 (1999) 274–284.
[30] K. Simons, E. Ikonen, Functional rafts in cell membranes, Nature 387 (1997) 569–572.
[31] K. Simons, D. Toomre, Lipid rafts and signal transduction, Nat. Rev. Mol. Cell Biol. 1 (2000) 31–39.
[32] M.F. Hanzal-Bayer, J.F. Hancock, Lipid rafts and membrane traffic, FEBS Lett. 581 (2007) 2098–2104.
[33] S.A. Jayasinghe, R. Langen, Lipid membranes modulate the structure of islet amyloid polypeptide, Biochemistry 44 (2005) 12113–12119.
[34] R.P. Nanga, J.R. Brender, S. Vivekanandan, A. Ramamoorthy, Structure and membrane orientation of IAPP in its natively amidated form at physiological pH in a membrane environment, Biochim. Biophys. Acta 1808 (2011) 2337–2342.
[35] R.P. Nanga, J.R. Brender, J. Xu, K. Hartman, V. Subramanian, A. Ramamoorthy, Three-dimensional structure and orientation of rat islet amyloid polypeptide protein in a membrane environment by solution NMR spectroscopy, J. Am. Chem. Soc. 131 (2009) 8252–8261.
[36] P.K. Mandal, J.W. Pettegrew, Alzheimer's disease: soluble oligomeric Abeta(1-40) peptide in membrane mimic environment from solution NMR and circular dichroism studies, Neurochem. Res. 29 (2004) 2267–2272.
[37] M. Coles, W. Bicknell, A.A. Watson, D.P. Fairlie, D.J. Craik, Solution structure of amyloid beta-peptide(1-40) in a water–micelle environment. Is the membrane-spanning domain where we think it is? Biochemistry 37 (1998) 11064–11077.

[38] C. Sizun, F. Aussenac, A. Grelard, E.J. Dufourc, NMR methods for studying the structure and dynamics of oncogenic and antihistaminic peptides in biomembranes, Magn. Reson. Chem. 42 (2004) 180–186.
[39] L. Khemtémourian, M.F. Engel, R.M. Liskamp, J.W.M. Höppener, J.A. Killian, The N-terminal fragment of human islet amyloid polypeptide is non-fibrillogenic in the presence of membranes and does not cause leakage of bilayers of physiologically relevant lipid composition, Biochim. Biophys. Acta 1798 (2010) 1805–1811.
[40] M.D. Kirkitadze, M.M. Condron, D.B. Teplow, Identification and characterization of key kinetic intermediates in amyloid beta-protein fibrillogenesis, J. Mol. Biol. 312 (2001) 1103–1119.
[41] H. Shao, S. Jao, K. Ma, M.G. Zagorski, Solution structures of micelle-bound amyloid beta-(1-40) and beta-(1-42) peptides of Alzheimer's disease, J. Mol. Biol. 285 (1999) 755–773.
[42] M.A. Sani, J.D. Gehman, F. Separovic, Lipid matrix plays a role in Abeta fibril kinetics and morphology, FEBS Lett. 585 (2011) 749–754.
[43] R. Soong, J.R. Brender, P.M. Macdonald, A. Ramamoorthy, Association of highly compact type II diabetes related islet amyloid polypeptide intermediate species at physiological temperature revealed by diffusion NMR spectroscopy, J. Am. Chem. Soc. 131 (2009) 7079–7085.
[44] M.F. Sciacca, J.R. Brender, D.K. Lee, A. Ramamoorthy, Phosphatidylethanolamine enhances amyloid fiber-dependent membrane fragmentation, Biochemistry 51 (2012) 7676–7684.
[45] K. Yuyama, K. Yanagisawa, Sphingomyelin accumulation provides a favorable milieu for GM1 ganglioside-induced assembly of amyloid beta-protein, Neurosci. Lett. 481 (2010) 168–172.
[46] E.E. Ambroggio, D.H. Kim, F. Separovic, C.J. Barrow, K.J. Barnham, L.A. Bagatolli, G.D. Fidelio, Surface behavior and lipid interaction of Alzheimer beta-amyloid peptide 1-42: a membrane-disrupting peptide, Biophys. J. 88 (2005) 2706–2713.
[47] M.S. Lin, H.M. Chiu, F.J. Fan, H.T. Tsai, S.S. Wang, Y. Chang, W.Y. Chen, Kinetics and enthalpy measurements of interaction between beta-amyloid and liposomes by surface plasmon resonance and isothermal titration microcalorimetry, Colloids Surf. B Biointerfaces 58 (2007) 231–236.
[48] L. Pieri, M. Bucciantini, P. Guasti, J. Savistchenko, R. Melki, M. Stefani, Synthetic lipid vesicles recruit native-like aggregates and affect the aggregation process of the prion Ure2p: insights on vesicle permeabilization and charge selectivity, Biophys. J. 96 (2009) 3319–3330.
[49] X. Yu, J. Zheng, Cholesterol promotes the interaction of Alzheimer beta-amyloid monomer with lipid bilayer, J. Mol. Biol. 421 (2012) 561–571.